Defect-Induced Photoconductivity in Layered Manganese Oxides: A Density Functional Theory Study

Kideok D. Kwon,[1,*] Keith Refson,[2] and Garrison Sposito[1]

[1]*Geochemistry Department, Earth Sciences Division, Lawrence Berkeley National Laboratory, Berkeley, California 94720, USA*

[2]*STFC Rutherford Appleton Laboratory, Didcot, Oxfordshire OX11 0QX, United Kingdom*

(Received 5 October 2007; published 7 April 2008)

Enhanced photoconductivity of layered Mn(IV)O_2 containing protonated Mn(IV) vacancy defects has been recently demonstrated, suggesting new technological possibilities for photoelectric conversion based on visible light harvesting. Using spin-polarized density functional theory, we provide the first direct evidence that such defects can indeed facilitate photoconductivity by (i) reducing the band-gap energy and (ii) separating electron and hole states. Our results thus support the proposition that nanosheet MnO_2 offers an attractive new material for a variety of photoconductivity applications.

DOI: 10.1103/PhysRevLett.100.146601 PACS numbers: 72.40.+w, 61.72.Bb, 61.72.uj, 73.22.−f

Manganese oxide nanosheets have emerged recently as interesting new materials for a host of potential applications in energy storage, electrochromism, and catalysis [1–5]. The desirable properties of these materials derive mainly from their nanosheet structure [1–6], which allows inexpensive manufacture, the use of flexible substrates, and facile shaping to suit a variety of devices. An important characteristic of the nanosheets in all materials synthesized thus far is the presence of cation vacancies ($Mn_{1-x}\square_xO_2$, where $\square_x$ represents a Mn vacancy) whose negative charge is typically compensated by interlayer metal cations or protons. Vacancies in metal oxides are well known to function as electron donors or acceptors, thereby enhancing material conductivity [7–10], and a similar role of the vacancies in Mn oxide nanosheets is possible.

Sakai *et al.* [6] recently reported the first observation of photocurrent generation by a Mn oxide. Protonated nanosheets were exfoliated from a digestion product containing approximately 3 mol% vacancies ($H_{0.13}[Mn(IV)_{0.97}\square_{0.03}]O_2$, mean Mn oxidation number 3.87 [1]). A monolayer film produced photocurrents under visible light radiation ($\lambda < 500$ nm) without significant structural decomposition [6]. Sakai *et al.* [6] speculated that the nanoscale thickness (<1 nm) of the film facilitated excited electron and hole escape before their recombination could occur.

Understanding electronic structure near the band gap of protonated Mn oxides is clearly essential to developing the full potential of these materials for harvesting visible light. In this Letter, we use spin-polarized density functional theory (DFT) to show that a Mn(IV) vacancy compensated by protons both narrows the energy gap between occupied and unoccupied electronic states of Mn oxides and separates photoinduced charge carriers effectively, thereby enhancing photoconductivity.

Protonated Mn vacancies in Mn(IV) oxides are known in the literature as Ruetschi defects [11]. Balachandran *et al.* [12] have reviewed the properties of Ruetschi defects and examined their impact on the structures of a number of MnO_2 polymorphs, including a layered variety. Using DFT with electron correlations described by the generalized gradient approximation (GGA), they found that a Ruetschi defect tends to stabilize MnO_2 polymorphs, especially those having more open structures featuring tunnels formed by chains of edge-sharing octahedra linked by shared corners (e.g., ramsdellite [13]). A similar type of defect in TiO_2, i.e., a Ti(IV) vacancy charge-compensated with four protons, has been observed and predicted to be a stable entity [14,15].

In the present study, we applied DFT to investigate the impact of a Ruetschi defect on the structure and electronic properties of a MnO_2 nanosheet bearing 0.033 and 0.125 Mn vacancies per octahedron. Vacancy-free Mn(IV)O_2, which has not yet been synthesized in the laboratory, was modeled based on published Mn and O atomic coordinates for a microcrystalline variety of layered MnO_2 (space group $P6_3/mmc$, $a = b = 2.840$ Å, $c = 14.031$ Å) prepared by thermal decomposition of $KMnO_4$ at 800 °C [16]. The Ruetschi defect was incorporated in MnO_2 supercells by coordination of one Mn vacancy at the center of each supercell to four H on "dangling" O ions around the vacancy. Two different defect concentrations were modeled, with one Mn vacancy placed in either a $4 \times 4 \times 1$ (32 Mn atoms) or a $2 \times 2 \times 1$ (8 Mn atoms) supercell, corresponding to the structural formulas, $H_{0.13}[Mn_{0.967}\square_{0.033}]O_2$ and $H_{0.50}[Mn_{0.875}\square_{0.125}]O_2$, respectively.

All DFT calculations were performed using the CASTEP code [17], with either the local spin density approximation (LSDA) or spin-polarized GGA/Perdew, Burke, and Ernzerhof (PBE) functionals [18], assuming ferromagnetic ordering among Mn ions [19]. For Mn and O, ultrasoft pseudopotentials [20] were constructed using the on-the-fly pseudopotential generator implemented in CASTEP, with valence electron configurations of $3s^23p^63d^54s^2$ with a core radius (r_c) of 2.3 a_0 for Mn and $2s^22p^4$ with

$r_c = 1.3\ a_0$ for O. Tests of the pseudopotentials at a 500 eV cutoff energy under LSDA reproduced structure and energy data for MnO calculated with the all-electron method [21]. For the first Brillouin zone, $6 \times 6 \times 2$, $5 \times 5 \times 2$, and $2 \times 2 \times 1$ k-point grids [22] were used for a vacancy-free MnO_2, a $2 \times 2 \times 1$ defect supercell, and a $4 \times 4 \times 1$ defect supercell, respectively. Tests of Brillouin zone sampling with the 500 eV cutoff energy showed very high convergence of force (0.01 eV/Å or better) and stress (0.01 Gpa or much better). For the Ruetschi-defected supercells, the three unit-cell angles (90°, 90°, and 120°), and the c-axis lattice parameters (13.892 Å in LSDA and 14.001 Å in GGA/PBE) were fixed based on optimized all-relaxed vacancy-free MnO_2 structures, but the other lattice parameters and all internal ionic positions were relaxed. Residual force and stress for the geometry-optimized structures with a 500 eV cutoff energy were less than 0.01 eV/Å and 0.02 GPa, respectively.

Table I shows that our LSDA and GGA/PBE optimizations closely bracket available experimental lattice parameters and Mn-O bond distances for layered MnO_2 with defects, in accordance with the usual DFT trend. In Ruetschi-defected MnO_2, the four H formed covalent bonds with coordinating O (O_H) (OH distance 0.984 to 1.001 Å) and hydrogen bonds with the O bound to two Mn (O_{2Mn}) (O-H...O_{2Mn} distance 1.96 to 2.17 Å) near the vacancy, such that the resulting OH groups were oriented to make a small angle (4° to 10°) with respect to the a-b plane. The interatomic distances between H are very short: 1.640 Å (LSDA) and 1.732 Å (GGA/PBE) in the $2 \times 2 \times 1$ supercells and 1.773 Å (LSDA) and 1.878 Å (GGA/PBE) in the $4 \times 4 \times 1$ supercells. Several possible H arrangements were explored by calculating total energies, with H thereby found to coordinate preferentially with O_{2Mn} (as would be expected from Pauling's rules) and to come into close proximity to one another. Similar structures were reported by Balachandran *et al.* [12].

Figure 1 compares the electronic density of states (DOS) of vacancy-free MnO_2 with Ruetschi-defected MnO_2. Incorporation of a Ruetschi defect significantly reduced the band-gap energy, from 1.3 eV to 0.9 eV in the $4 \times 4 \times 1$ supercell and from 1.3 eV to 0.3 eV in the $2 \times 2 \times 1$ supercell (GGA/PBE). Sakai *et al.* [6] reported an indirect band-gap energy of 2.23 eV for the Mn oxide nanosheets they prepared, based on a relationship between the incident photon energy and the incident photon-to-current efficiency. It is well known that LDA and GGA generally underestimate band gaps of semiconductors. However, for insulating and semiconducting systems, the primary effect of this DFT underestimation is a uniform downward shift of all conduction bands. Our calculations demonstrate additional valence levels for systems containing Ruetschi defects, so the band-gap shift is modeled fairly reliably even though the absolute value is not. Improved band-gap energy estimates may be obtained with the DFT + U approach [24] or the screened exchange method [25].

The substantial reduction in band-gap energy we observed is due to the introduction of states at the top of the valence band (VB) (arrows in Fig. 1) by the Ruetschi defect. Detailed orbital analysis revealed that these newly introduced states around −1 to 0 eV are contributed almost entirely by nearest-neighbor Mn and O ions around the cation vacancy. In particular, the localized states were mostly Mn-3d states and O_{2Mn}-p states around the Ruetschi defect. The O_{2Mn}-p states were oriented parallel to the axial Mn-O bonds in the MnO_6 octahedra and are a consequence of Mn-O bonds lost by removal of Mn^{4+}, which results in dangling states that are analogous to nonbonding states compared to O_H (at around −8 eV in Fig. 1) or to saturated O bound to three Mn atoms (O_{3Mn}). The O_{2Mn} states are reflected also in the noticeable induction of spin polarization on the O_{2Mn}; the magnetic moment increases from $-0.04\mu_B$ on O_{3Mn} in vacancy-free MnO_2 to between $+0.12\mu_B$ and $+0.14\mu_B$ on the O_{2Mn} (GGA/PBE).

According to our DFT calculations, the Mn-3s states were strongly polarized, leading to significant energy splitting (ΔE_{Mn3s}) between the spin-up and spin-down states of Mn-3s. Our values of ΔE_{Mn3s} can be compared to the

TABLE I. Interatomic distances in vacancy-free and Ruetschi-defected MnO_2 optimized with spin-polarized DFT. Vacancy rate per octahedron indicated at the top of each column of data. Values in parentheses are averages of calculated interatomic distances.

	LSDA			GGA/PBE			Experimental			
Distance (Å)	0	0.033	0.125	0	0.033	0.125	0.03[a]	0.03[b]	0.06[c]	0.12[d]
Mn_{layer}-Mn_{layer}	2.827	2.756–2.888 (2.825)	2.815	2.897	2.820–2.943 (2.895)	2.895	2.85	2.86	2.88	2.840
Mn_{layer}-O_{layer}	1.883	1.833–1.929 (1.882)	1.854–1.929 (1.882)	1.925	1.852–2.002 (1.928)	1.887–1.979 (1.931)	1.91	1.89	1.90	1.914
Mn sheet thickness	1.88	1.91	1.98	1.91	1.94	2.02				1.96

[a]Mn K-edge EXAFS analysis (±0.01 Å) of protonated nanosheet MnO_2, $H_{0.13}[Mn(IV)_{0.87}\square_{0.03}]O_2 \cdot 0.7H_2O$ [2]. The Mn-Mn distance is 2.842 Å by x-ray diffraction (XRD) analysis.
[b]Mn K-edge EXAFS analysis of protonated nanosheet MnO_2 [3].
[c]Mn K-edge EXAFS analysis (±0.02 Å) of nanoparticle δ-MnO_2, $Na_{0.24}[Mn(IV)_{0.94}\square_{0.06}]O_2 \cdot 0.72H_2O$ [23]. The Mn-O distance is 1.92 Å by XRD analysis.
[d]XRD analysis of microcrystalline layered K-MnO_2, $K_{0.231}Mn(III)_{0.077}[Mn(IV)_{0.885}\square_{0.115}]O_2 \cdot 0.60H_2O$ [16]. The Mn-Mn distance for a powder sample was 2.845 Å by XRD analysis and 2.87 Å by Mn K-edge EXAFS analysis.

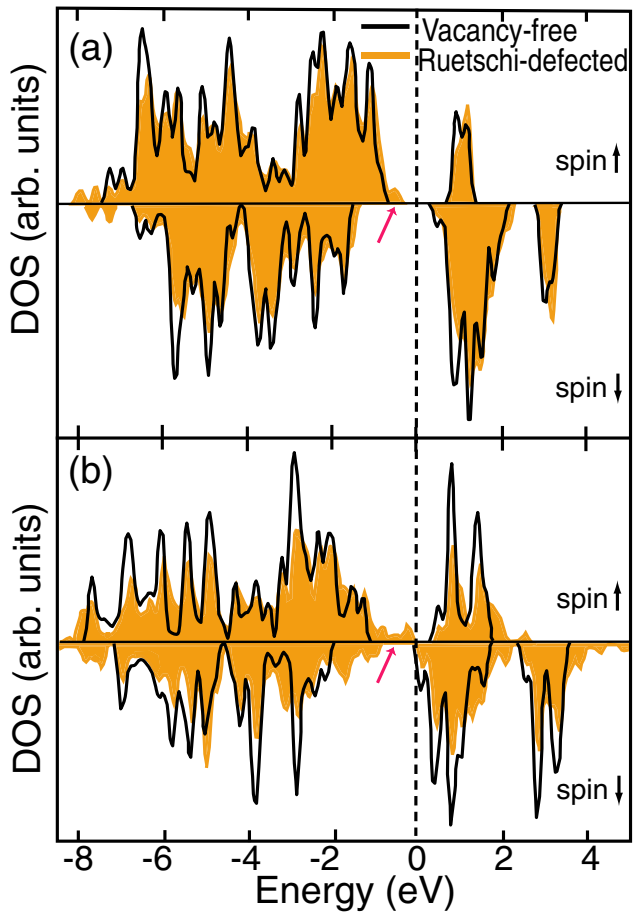

FIG. 1 (color online). Density of states (DOS) of vacancy-free MnO_2 and Ruetschi-defected MnO_2 in (a) the $4 \times 4 \times 1$ supercell and (b) the $2 \times 2 \times 1$ supercell for spin-up (↑) and spin-down (↓) states. The Fermi energy of Ruetschi-defected MnO_2 was set equal to zero. The conduction band minimum (CBM) of vacancy-free MnO_2 was aligned at the CBM of Ruetschi-defected MnO_2. The slight occupation above E_F in the $2 \times 2 \times 1$ supercell is due to Gaussian smearing of the DOS over the 0.05 eV width.

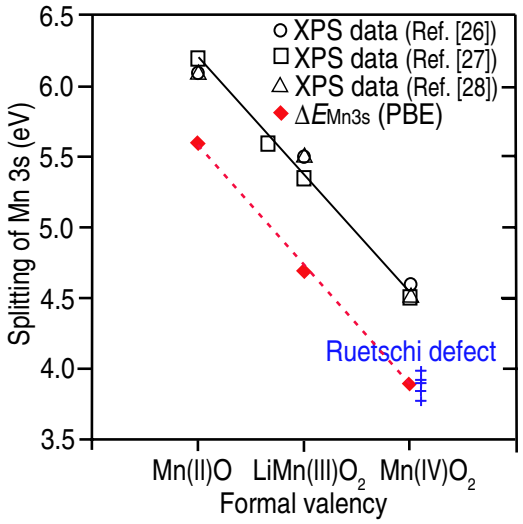

FIG. 2 (color online). Calculated Mn-3s splitting (ΔE_{Mn3s}) for Mn ions in MnO, $LiMnO_2$, vacancy-free MnO_2, and Ruetschi-defected MnO_2. Experimental data are for MnO, Mn_2O_3, and β-MnO_2 (Refs. [26,28]) and MnO, Mn_3O_4, $LiMnO_2$, and Li_2MnO_3 (Ref. [27]). Cubic MnO and monoclinic $LiMnO_2$ splittings were also calculated with spin-polarized GGA/PBE and ferromagnetic ordering among Mn ions. Solid and dash lines guide the data trends.

Mn-3s spectral splitting as measured by x-ray photoelectron spectroscopy, which has been used to identify formal Mn valence states [26,27]. The GGA/PBE results underestimate ΔE_{Mn3s}, but they do so in a systematic way (Fig. 2) when compared to experimental Mn-3s splittings [26–28]. The calculated ΔE_{Mn3s} values are 3.9 eV for vacancy-free MnO_2 and 3.8 to 4.0 eV for Ruetschi-defected MnO_2. This very slight change indicates that the influence of Ruetschi defects on the magnetic moments of the Mn atoms around the defect sites is quite minor, so a formal high-spin Mn (IV) state can be assigned to the Mn ions in both vacancy-free and Ruetschi-defected MnO_2.

Figure 3 shows that Ruetschi defects reduce the band-gap energy effectively both for the yield in electron-hole pair formation and for charge carrier mobility under photon illumination. In vacancy-free MnO_2, the fundamental band gap is indirect [Fig. 3(a)], and light absorption would typically be weak. Introduction of a direct excitation at Γ by the Ruetschi defect [Fig. 3(b)] should enhance light absorption compared to vacancy-free MnO_2. On the other hand, band-gap-reducing states often diminish the photoactivity of materials because, localized deep inside the band gap, they often function as recombination centers, or traps, of photogenerated electrons and holes (e.g., d states of transition metals doped into TiO_2) [29]. In the design of solar cell applications of semiconductors, efficient separation of photoinduced charge carriers has been a principal goal [30]. The states introduced in Ruetschi-defected MnO_2 have a finite bandwidth overlapping the band states of MnO_2, and the change in the conduction band (CB) from the defect is negligible [Figs. 3(a) and 3(b)]. Therefore, band-gap reduction by Ruetschi defects would not lower the mobility of the photoproduced charge carriers. This point is seen clearly in comparing the charge distribution (orbitals) at the valence band maximum (VBM) and the conduction band minimum (CBM) for vacancy-free MnO_2 and Ruetschi-defected MnO_2 [Figs. 3(c) and 3(d)]. In the vacancy-free MnO_2, most of electron and hole states are overlapping, whereas in the Ruetschi-defected MnO_2, the electron and hole states are well separated. The VBM hole states are near the vacancy site, and the CBM electron states are mostly in a neighboring sheet well away from the VBM hole states. The lowest CB electron states near the vacancy site are found at *ca.* 0.2 eV ($4 \times 4 \times 1$ supercell) and 0.3 eV ($2 \times 2 \times 1$ supercell) above the CBM at Γ of the Ruetschi-defected MnO_2.

In summary, the results presented here show that a Ruetschi defect in nanosheet MnO_2 effectively reduces

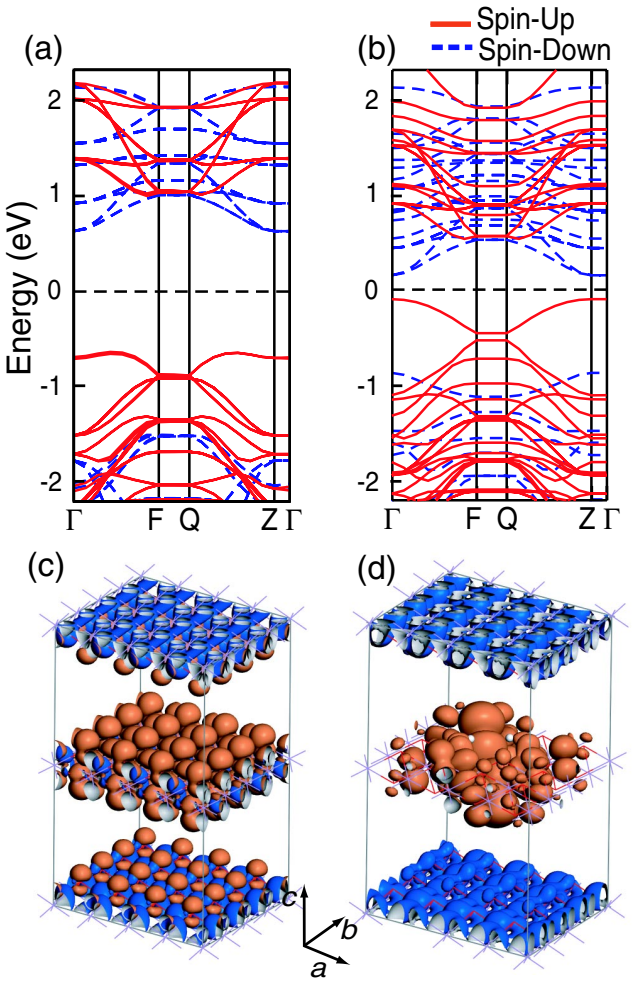

FIG. 3 (color online). [H: white, Mn: purple (or dark gray), O: red (or lightest gray)] Band structures of (a) vacancy-free MnO_2 and (b) Ruetschi-defected MnO_2 ($2 \times 2 \times 1$ supercell). Views of charge distributions of valence band maximum (VBM) hole states [orange (or light gray)] and conduction band minimum (CBM) electron states [blue (or gray)] in (c) vacancy-free MnO_2 and (d) its Ruetschi-defected MnO_2 ($4 \times 4 \times 1$ supercell). The Fermi energy was set equal to zero. Isosurfaces represent 0.001 $e^-/Å^3$.

the band-gap energy between occupied and unoccupied electronic states relative to a defect-free layered Mn oxide. Our finding of enhanced photoconductivity by introducing Ruetschi defects suggests that photoinduced electronic transitions by nanosheet MnO_2 can be optimized by control of defect formation rates during the synthesis of these self-doped materials.

This research reported in this Letter was supported by the Director, Office of Energy Research, Office of Basic Energy Sciences, of the U.S. Department of Energy under Contract No. DE-AC03-76SF00098. Our computations used resources of the National Energy Research Scientific Computing Center, which is supported by the Office of Science of the U.S. Department of Energy under Contract No. DE-AC02-05CH11231. We also acknowledge the use of the SCARF computing facilities at STFC Rutherford Appleton Laboratory.

*Corresponding author.
kkwon@nature.berkeley.edu

[1] Y. Omomo *et al.*, J. Am. Chem. Soc. **125**, 3568 (2003).
[2] K. Fukuda *et al.*, J. Phys. Chem. B **110**, 17 070 (2006).
[3] Y. Kadoma, Y. Uchimoto, and M. Wakihara, J. Phys. Chem. B **110**, 174 (2006).
[4] N. Sakai *et al.*, J. Electrochem. Soc. **152**, E384 (2005).
[5] K. Izawa *et al.*, J. Phys. Chem. B **110**, 4645 (2006).
[6] N. Sakai *et al.*, J. Phys. Chem. B **109**, 9651 (2005).
[7] I. Justicia *et al.*, Adv. Mater. **14**, 1399 (2002).
[8] I. S. Elfimov, S. Yunoki, and G. A. Sawatzky, Phys. Rev. Lett. **89**, 216403 (2002).
[9] H. Y. Hwang, Nat. Mater. **4**, 803 (2005).
[10] M. Nolan and S. D. Elliott, Phys. Chem. Chem. Phys. **8**, 5350 (2006).
[11] P. Ruetschi, J. Electrochem. Soc. **131**, 2737 (1984).
[12] D. Balachandran *et al.*, J. Solid State Chem. **173**, 462 (2003).
[13] J. E. Post, Proc. Natl. Acad. Sci. U.S.A. **96**, 3447 (1999).
[14] J. A. Wang *et al.*, J. Phys. Chem. B **105**, 9692 (2001).
[15] I. E. Grey and N. C. Wilson, J. Solid State Chem. **180**, 670 (2007).
[16] A. C. Gaillot *et al.*, Chem. Mater. **15**, 4666 (2003).
[17] S. J. Clark, M. D. Segall, C. J. Pickard, P. J. Hasnip, M. J. Probert, K. Refson, and M. C. Payne, Z. Kristallogr. **220**, 567 (2005).
[18] J. P. Perdew, K. Burke, and M. Ernzerhof, Phys. Rev. Lett. **77**, 3865 (1996).
[19] Antiferromagnetic alignment of Mn ions between sheets, with ferromagnetic ordering within each sheet, was also tested, but the energy difference found was less than the converged energy variability of the alternatives.
[20] D. Vanderbilt, Phys. Rev. B **41**, 7892 (1990).
[21] J. E. Pask *et al.*, Phys. Rev. B **64**, 024403 (2001).
[22] H. J. Monkhorst and J. D. Pack, Phys. Rev. B **13**, 5188 (1976).
[23] M. Villalobos *et al.*, Am. Mineral. **91**, 489 (2006).
[24] V. I. Anisimov, F. Aryasetiawan, and A. I. Lichtenstein, J. Phys. Condens. Matter **9**, 767 (1997).
[25] A. Seidl *et al.*, Phys. Rev. B **53**, 3764 (1996).
[26] J. S. Foord, R. B. Jackman, and G. C. Allen, Philos. Mag. A **49**, 657 (1984).
[27] V. R. Galakhov *et al.*, Phys. Rev. B **65**, 113102 (2002).
[28] G. K. Wertheim, S. Hüfner, and H. J. Guggenheim, Phys. Rev. B **7**, 556 (1973).
[29] W. Choi, A. Termin, and M. R. Hoffmann, J. Phys. Chem. **98**, 13 669 (1994).
[30] M. Grätzel, Nature (London) **414**, 338 (2001).